JOURNAL OF MATERIALS SCIENCE 28 (1993) 5863–5868

Effect of heat treatment on the structure and hardness of FeCrNiAl alloys

S. YAMADA, T. HAMADA, J. IMAI
Material Research and Development Laboratory, Matsushita Electric Works Ltd 1048 Kadoma, Osaka 571, Japan

Y. KAWAMURA, T. SABURI
Department of Material Science and Engineering, Osaka University, Yamadaoka 2-1, Suita, Osaka 565, Japan

Heat treatment of the Fe–35Cr–21Ni–6.7Al–0.3Zr alloy results in the formation of an alumina layer on its surface. The NiAl-based B2 phase particles in this alloy change their dispersion state according to the heat treatment conditions. Structural and hardness changes of the alloy were examined for specimens heat-treated at a temperature between 1323 and 1523 K for 0.3 to 54.0 ks followed by air cooling at a rate of 100 $K s^{-1}$. Three sizes of B2 phase particles were observed, i.e. particles of several micrometres, 100 to 300 nm and a few dozen nanometres; the thickness of the alumina layer on the surface increased with heating time. The particles of several micrometres disappeared from the near-surface region as the heat treatment proceeded, and instead finely dispersed B2 particles of 100 to 300 nm or a few dozen nanometres appeared after fast cooling from the heat-treatment temperature. Thus, the matrix hardness increased with heating time and heating temperature, since more fine particles were obtained.

1. Introduction

Recently, various attempts have been made to improve the hardness and wear resistance of metals by forming oxide, nitride or other substances on the surface of the metals. Available methods include (i) those in which oxide or nitride is formed by physical vapour deposition (PVD), chemical vapour deposition (CVD) or other methods, and (ii) those in which oxide or nitride is formed on the surface of the metal by plasma spraying [1, 2]. The former methods are not appropriate in that the film thickness obtained is usually less than 1 μm, too thin for this purpose, and the cohesion between the surface film and the matrix is weak. The latter method presents difficulties in accurate control of film thickness in a range of the order of 100 μm, in that the material is exposed to heat, and also the cohesion of the surface layer is weak. Thus, at present it is difficult to fix a ceramic material of 1 to 20 μm thickness on the surface of metal with sufficient cohesion using state-of-the-art techniques. Given this situation, we explored a new method using an FeCrNiAl alloy [3, 4], resulting from nickel supplementation of an FeCrAl alloy [5–11], and developed it as an oxidation-resistant material. In this method the alloy surface is oxidized in air to form an alumina layer, with the aim of developing a hard, wear-resistant surface. Although this alloy is basically characterized by a body-centred cubic α phase, a fraction of austenite, depending on the compositional variation and the dispersion state of the B2 intermetallic compound, changes during the oxidation treatment, resulting in changes in its hardness [4]. When we apply this alloy as a material for cutting tools or wear-resistant parts, the matrix (the internal portion, as against the alumina formed on the material surface) is itself required to be sufficiently hard and strong. Thus in the present study, changes in structures and hardness were examined for various oxidation conditions of the FeCrNiAl alloy.

2. Experimental procedure

The subject alloy was prepared by melting electrolytic iron (over 99.9 wt %), electrolytic chromium (over 99.8 wt %), electrolytic nickel (over 99.8 wt %), an FeAl-base alloy (composition 50:50 wt %, purity over 99.47 wt %) and an FeZr-base alloy (composition 23.5:76.5 wt %, purity over 99.8 wt %). All were weighed out in an alumina crucible, melted using a high-frequency melting furnace, and the melt was cast in a copper crucible. A vacuum of 1.3×10^{-3} Pa was maintained during melting. The alloy was analysed for composition using an inductively coupled plasma (ICP) emission spectrometer. The blending ratio and analytical data are given in Table I. The cast ingot thus obtained was repeatedly hot-rolled to a 0.1 mm thick plate, which was subjected to three cycles of ultrasonic cleaning in acetone to yield a sample.

The sample was subjected to heat treatment in an electric furnace in air at 1323 to 1523 K, which was reached at a heating rate of 6 $K s^{-1}$, for 0.3 to 54 ks. This was followed by cooling in outside air at a rate of

0022–2461 © *1993 Chapman & Hall*

TABLE I Prescribed and analysed compositions of the alloy (wt %)

	Cr	Ni	Al	Zr	Fe
Prescribed	35.0	21.0	6.7	0.3	Bal.
Analysed	34.5	21.4	6.4	0.31	Bal.

about 100 K s^{-1}. Structural observation was carried out using a light microscope, a scanning electron microscope (SEM) (Jeol JXA-733) and a transmission electron microscope (TEM) (Hitachi H-800, acceleration voltage 200 kV). Light microscopic specimens were prepared by polishing a cross-section of the sample using SiC paper and then using diamond paste to 6 μm and then 1 μm followed by etching with Vilella reagent (HNO_3:HCl:glycerol = 1:2:3) for 30 s. SEM specimens were prepared by polishing the sample using SiC paper and diamond. TEM specimens were prepared by jet-polishing the sample with 10% perchloric acid and 90% glacial acetic acid at a liquid temperature of 303 K.

The alumina layer thickness was obtained by taking an average of a few dozen measuring points at equal intervals on the alumina layer on a cross-sectional micrograph.

3. Results and discussion

3.1. Formation of B2 phase particles

The as-hot rolled sample (0.1 mm thick) was subjected to X-ray diffraction analysis of its surface to identify the phases constituting it. Fig. 1 shows the X-ray diffraction pattern obtained, which demonstrates that the sample is comprised of an α phase with a body-centred cubic structure and an intermetallic compound with a B2 structure. The sample heat-treated at 1423 K for 3.6 ks and then air-cooled was examined by TEM for particle size and shape. Fig. 2 shows a dark-field image and the diffraction pattern obtained. The diffraction pattern shows weak spots of the B2 intermetallic compound as well as strong spots of the matrix α phase, such as at 1 1 0, 2 0 0 and 2 2 0. The dark-field image, taken with the 1 0 0 reflection of the B2 phase, reveals the presence of three sizes of B2 phase particles in the dispersion: particles of several micrometres, finer particles of 100 to 300 nm and some of a few dozen nanometres diameter. These B2 phase particles are not the 1:1 NiAl intermetallic compound but contain iron and chromium [4].

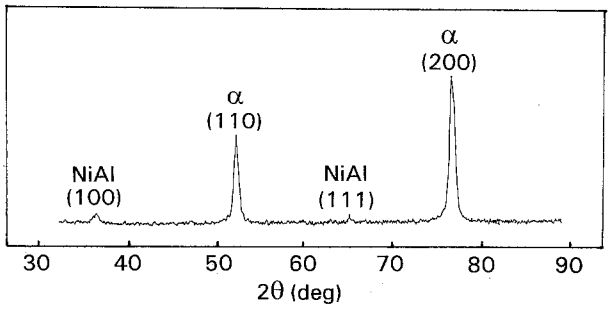

Figure 1 X-ray diffraction pattern obtained from the FeCrNiAl alloy.

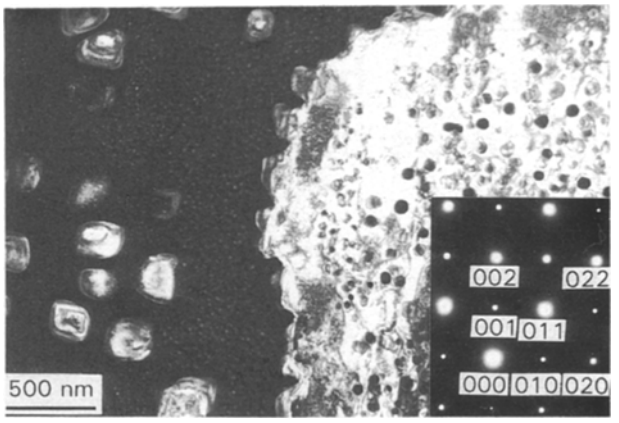

Figure 2 Dark-field TEM image by 1 0 0 reflection of the B2 phase and the corresponding electron diffraction pattern of the FeCrNiAl alloy (after heat treatment at 1423 K for 3.6 ks).

3.2. Differences in distribution scheme of the B2 phase particles due to heat treatment

Fig. 3 shows light microscopic images of cross-sections of samples heat-treated at 1423 K for various periods of time, i.e 0.3, 3.6, 14.4 and 54 ks. The black surface layer (the boundary between the sample and the embedding resin is shown by a white dotted line, since it is not easily visible) is the alumina layer formed on the surface during heat treatment. It appears as if it is rooted into the substrate. Dispersed in the substrate are NiAl-based B2 phase particles as described above. The B2 phase particles, which were of a thin plate-like shape (particles of several micrometres in diameter seen in the dark-field image in Fig. 2) in the as-hot rolled condition became slightly thicker after 0.3 ks as seen in (Fig. 3a), and became still thicker and more spherical after 3.6 ks as seen in (Fig. 3b). After 3.6 ks there appeared a region that was free from B2 phase particles of several micrometres, extending about 20 μm below the surface. This is attributable to dissolution of the NiAl-based B2 phase particles into the matrix, caused by a decrease in aluminium content due to formation of Al_2O_3 on the surface. After 14.4 ks (Fig. 3c) the B2 phase particles became still thicker and more spherical, while the region free of B2 phase particles extended. After 54 ks (Fig. 3d) this tendency became more pronounced, and in the vicinity of the surface lacking the ferrite-forming element aluminium, the austenite phase (the white portions under the surface alumina layer) appeared.

Fig. 4 shows the dependence of the width of the layer lacking B2 phase particles on heating temperature, and also on the holding time. At a constant temperature, the width of the particle-free layer increases almost linearly as a logarithmic function of time. Also, with increasing temperature from 1323 to 1423 K, and from 1448 to 1473 K, the rate of increase in the width of the particle-free layer increased with heating time. This finding can be explained as follows:

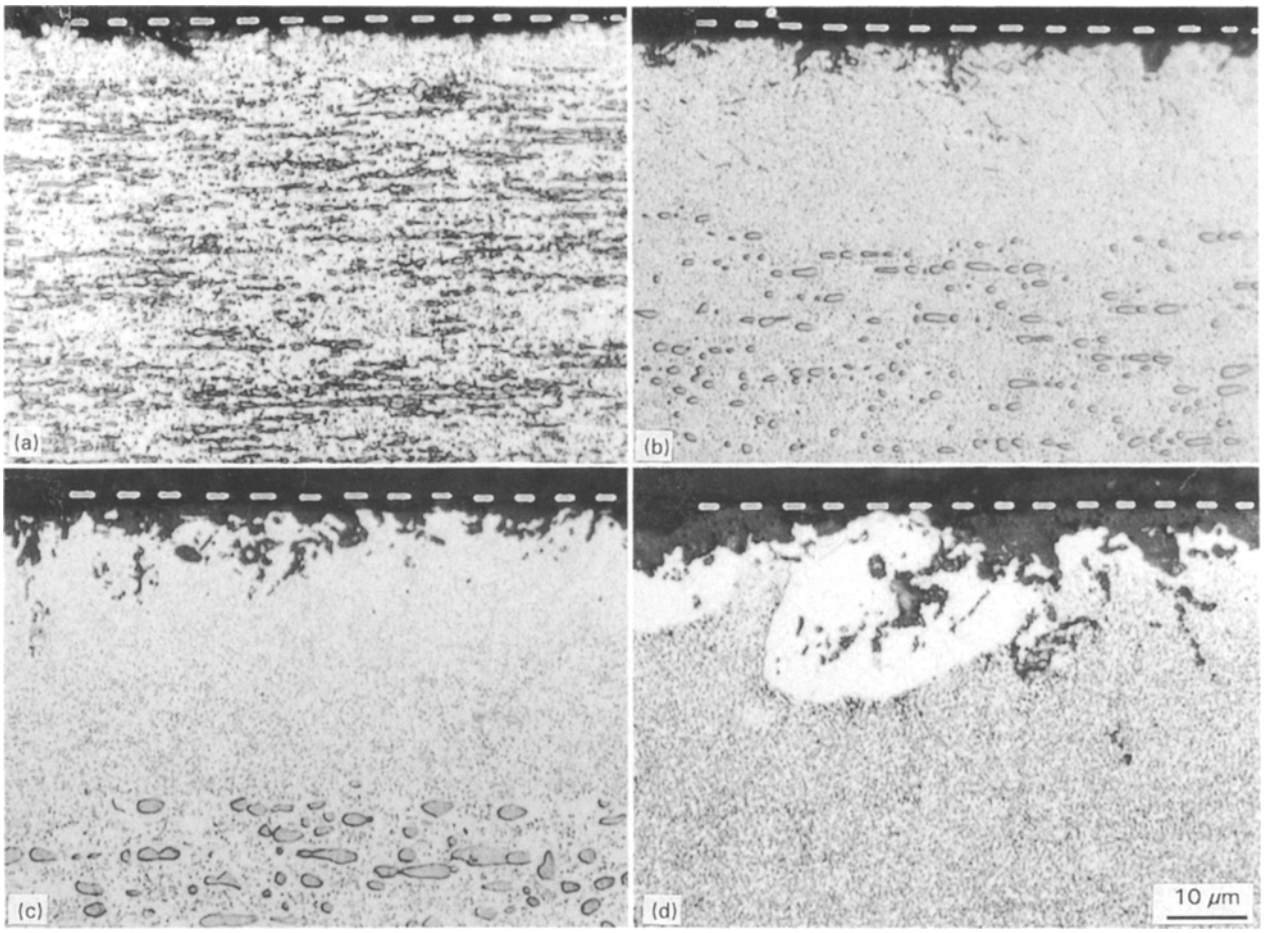

Figure 3 Structural changes with heating time at 1423 K: (a) 0.3 ks, (b) 3.6 ks, (c) 14.4 ks, (d) 54 ks.

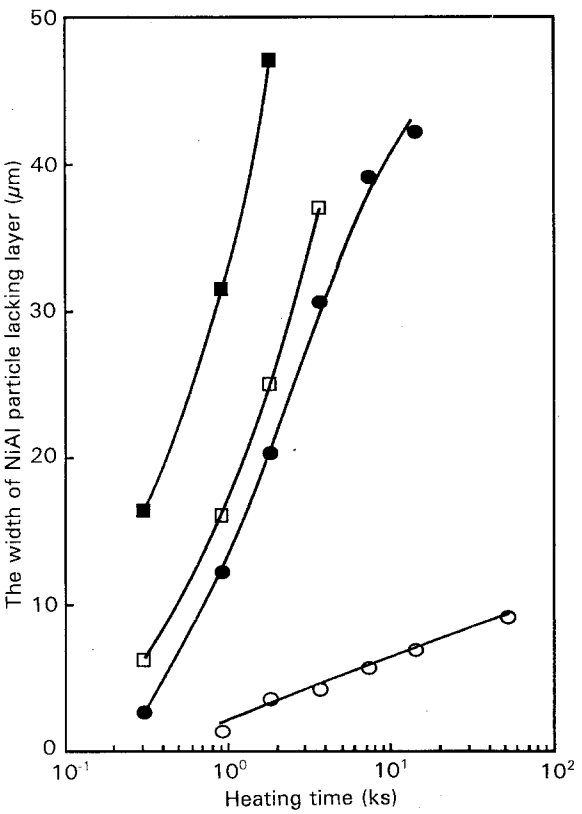

Figure 4 Relationship between the width of the layer lacking large NiAl particles and heating time at different temperatures: (○) 1323 K, (●) 1423 K, (□) 1448 K, (■) 1498 K.

as the heating temperature rises, the distance aluminium can travel increases because of the increase in the diffusion coefficient of oxygen in the alumina layer and also in the matrix, so that aluminium at deeper levels diffuses to the surface, which results in a lack of aluminium in that region and thus in an increase in the width of the layer lacking B2 phase particles.

3.3. Relation between alumina layer thickness and heat treatment

Fig. 5 shows the relationships between holding time at various heating temperatures and the thickness of the alumina layer formed. The thickness of the alumina layer increased with holding time. Also, the thickness of the alumina layer increased rapidly with heating temperature. This increase in the thickness had almost the same tendency as the increase in the thickness of the layer depleted of B2 phase particles with temperature shown in Fig. 4. This finding suggests that while aluminium diffuses to the surface to form an alumina layer, the B2 phase particles in the near-surface region dissolve in the matrix phase.

Fig. 6 shows SEM micrographs of cross-sections of the sample held at 1423 K for 3.6 ks (Fig. 6a) and 14.4 ks (Fig. 6b). Table II gives the result of X-ray micro analysis of the compositions at positions A, B, C and D in Fig. 6. The width of the layer free of B2 phase particles was 30 μm after a heating time of 3.6 ks and

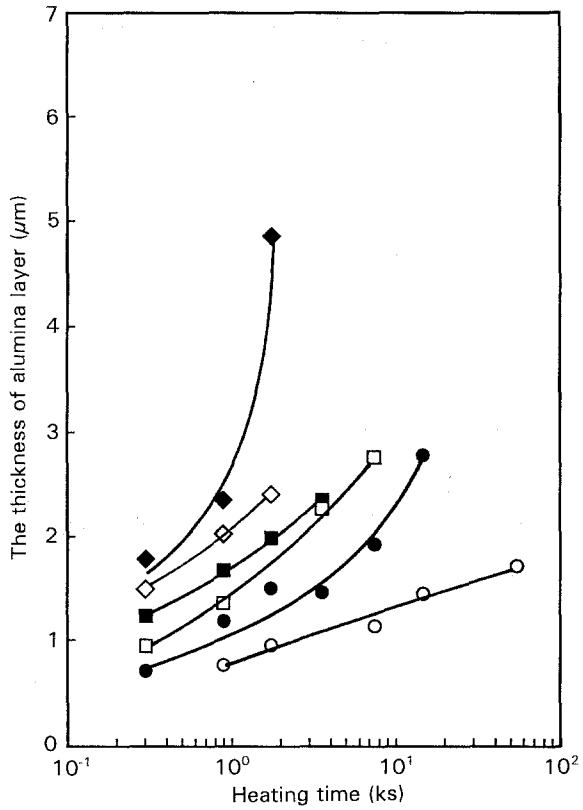

Figure 5 Dependence of the thickness of the alumina layer on heating time at different temperatures: (○) 1323 K, (●) 1423 K, (□) 1448 K, (■) 1473 K, (◇) 1498 K, (◆) 1523 K.

TABLE II Results of X-ray micro analysis on the compositions of the portions shown in Fig. 6

Measured area or point	Element (wt %)			
	Cr	Ni	Al	Fe
A	37.7	19.7	4.9	Bal.
B	37.4	19.9	4.8	Bal.
C	37.1	20.6	4.4	Bal.
D	37.2	20.7	4.3	Bal.

40 μm after 14.4 ks. The regions A and C are 15 μm square and were selected in the region free of B2 phase particles of several micrometres; the regions B and D were selected as circular regions of 2 μm diameter in between the particles in the particle-containing region. In the case of 3.6 ks heating time (Fig. 6a), regions A and B have a nearly equal aluminium content, lower by about 2 wt % than the average aluminium content in the ingot (6.4 wt % as shown in Table I). Thus 1.5 wt % aluminium is thought to have diffused to the surface to form alumina from the region A and to have been consumed to form NiAl-based B2 phase particles of several micrometres in the region B.

In the case of 14.4 ks heating time (Fig. 6b), regions C and D have a nearly equal aluminium content, lower by 2.0 wt % than the average aluminium content in the ingot. Since holding at 1423 K causes aluminium to diffuse to the surface and form alumina, the B2 phase particles of several micrometres, dispersed in the matrix in a hot-rolled state, disappear as

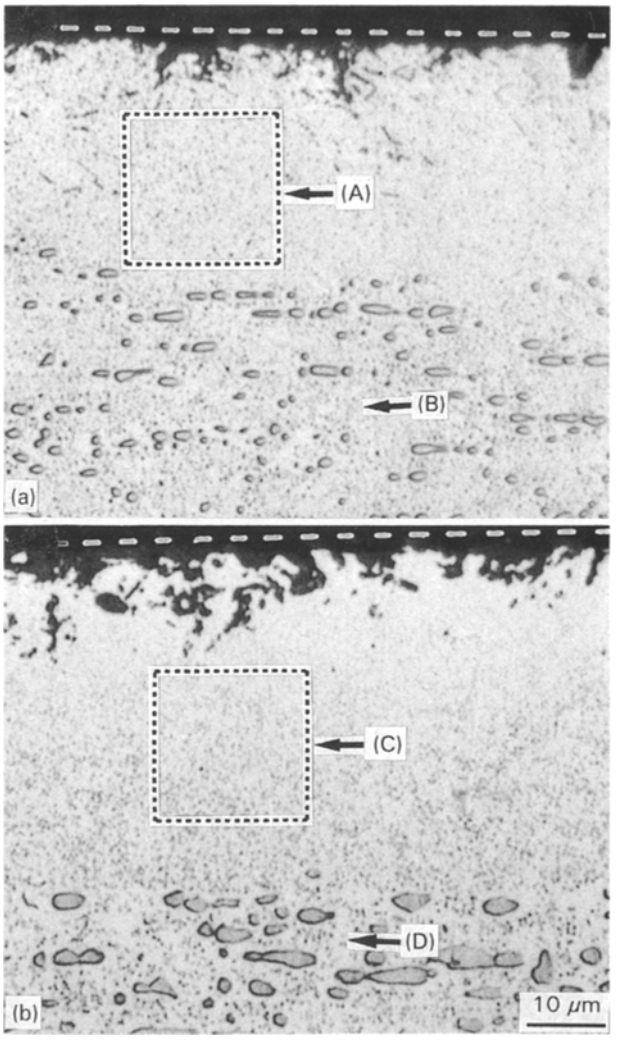

Figure 6 Changes in local composition after heating at 1423 K for (a) 3.6 ks, (b) 14.4 ks.

a result of their being consumed to compensate for the lack of aluminium. At the same time, more and more aluminium diffuses to the surface, resulting in a reduction of the aluminium content in the matrix. In the region in which NiAl-based B2 phase particles of several micrometres exist, the particle shape changes from plate-like to spherical with time, as mentioned before; the concurrent reduction in the aluminium content in the matrix decreases.

3.4. Relation between matrix hardness and heat treatment

Fig. 7 shows the relationship between heating time and the hardness of the matrix (mid-depth portion of the plate) at various heating temperatures. At 1323 K curve (a) the hardness remained almost unchanged even when the heating time was extended. At temperatures from 1423 to 1498 K curves (b) to (e) the hardness increased with heating time. The rate of increase in hardness with heating time increases with temperature, although it becomes small at 1523 K as seen in curve (f). The matrix hardness depends basically on the dispersion scheme of the three sizes of NiAl-based B2 phase particles described in Section 3.1 upon cooling after heat treatment. The dispersion scheme of

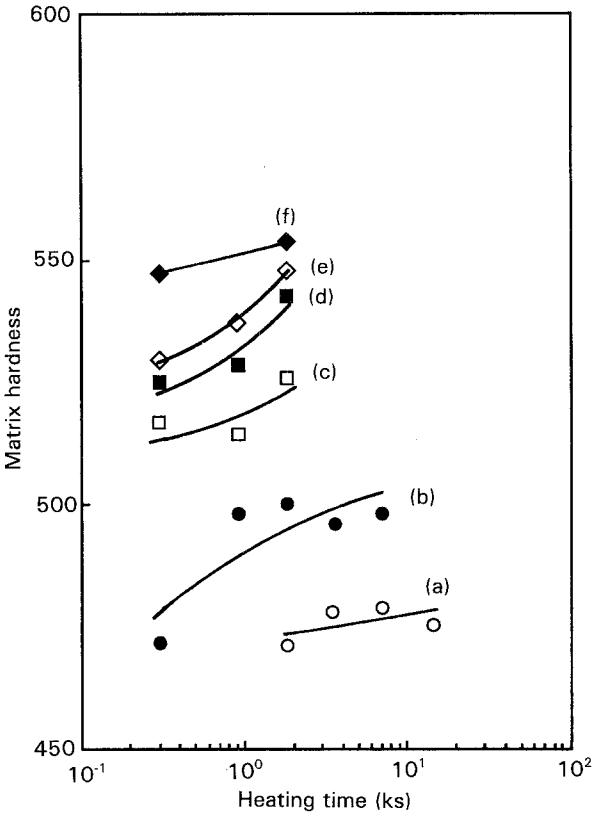

Figure 7 Relation between matrix hardness (H_V) and heat treatment at (a) 1323 K, (b) 1423 K, (c) 1448 K, (d) 1473 K, (e) 1498 K, (f) 1523 K.

the particles of a few dozen nanometres or of 100 to 300 nm appears to determine the hardness.

We interpret the relation between the hardness of the matrix and the heat treatment as follows. At 1323 K (curve (a) of Fig. 7), the NiAl-based B2 phase particles of several micrometres, originally dispersed in the sample, do not dissolve completely in the matrix even after a prolonged heating time, probably due to slow diffusion and also to a phase equilibrium. Thus, the fraction of nickel and aluminium in the matrix remain low, and the number of particles of a few dozen nanometres and of 100 and 300 nm is not sufficient to increase the matrix hardness. When the heating temperature is increased from 1423 to 1498 K, the B2 phase particles of several micrometres dissolve in the matrix when kept at these temperatures. The B2 phase particles dissolve with increasing holding time and with increasing heating temperature; therefore more B2 phase particles of a few dozen nanometres or 100 to 300 nm form upon cooling to increase the hardness. Thus, if the rate of cooling after the high-temperature holding is high enough, the hardness increases with holding time, and the rate of increase in the hardness increases with temperature. At 1523 K (curve (f)), B2 phase particles of several micrometres dissolve completely in the matrix in a short time due to the fast diffusion and also a large dissolution limit; therefore a large number of particles of a few dozen nanometres or 100 to 300 nm are dispersed to contribute to the increase in the hardness. Thus, the hardness increase occurs with a relatively short holding time and it is almost the same even when the heating time is extended.

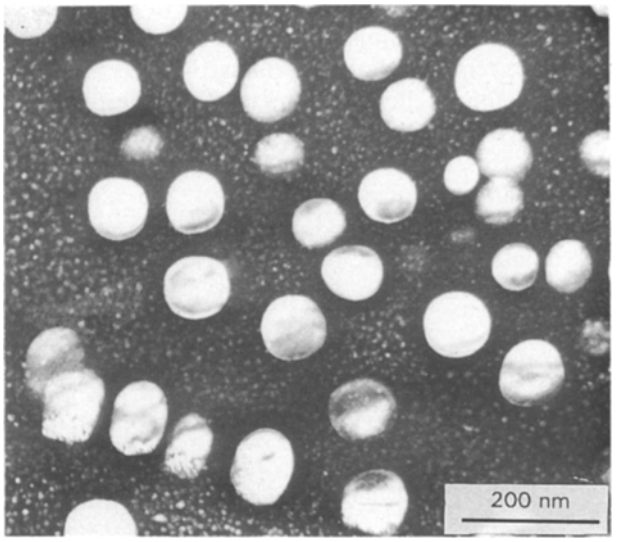

Figure 8 Dark-field TEM micrographs of fine (a few dozen nanometres, 100 to 300 nm) B2 phase particles after heat treatment at 1423 K for 7.2 ks, taken with the 1 0 0 superlattice reflection of the B2 phase.

Fig. 8 shows TEM micrographs of B2 phase particles of a few dozen nanometres and 100 to 300 nm after heat treatment at 1423 K for 7.2 ks. The matrix hardness appears to depend on the dispersion scheme of these particles of a few dozen nanometres or 100 to 300 nm, as stated above.

4. Conclusion

With respect to Fe–35Cr–21Ni–6.7Al–0.3Zr (by blending), the effect of heat treatment in air on its structure was examined and its relation to the hardness of the material was discussed. The findings are summarized as follows.

1. Depending on the heat treatment after hot rolling, three sizes of particles are formed: a few dozen nanometres, 100 to 300 nm and several micrometres, and the particles are of an NiAl-based intermetallic compound with a B2 structure.

2. Upon heat treatment, alumina forms on the surface. Its thickness increases with heating time. Concurrently, the NiAl-based B2 phase particles of several micrometres disappear in the region near the surface; the width of the layer lacking these particles increases with increasing heating time, and the rate of its increase increases with increasing heating temperature. This increase in the thickness of the alumina layer is similar in its tendency to the increase in the width of the layer lacking B2 phase particles. The disappearance of NiAl-based B2 phase particles of several micrometres from the near-surface region is attributed to a decrease in aluminium content due to the formation of surface alumina.

3. As for the matrix hardness, it remains almost unchanged ($H_V \simeq 470$) even after prolonged heating at a temperature below 1323 K. At temperatures between 1423 and 1498 K the hardness increases with

heating time, and the rate of increase in the hardness increases as a function of heating time. At 1523 K, the hardness remains almost unchanged ($H_V \simeq 550$) even after prolonged heating. This can be interpreted as follows; at temperatures above 1423 K, prolonged heating causes the B2 phase particles to dissolve in the matrix and to increase the nickel and aluminium contents in the matrix, which results in an increase in the number of fine B2 phase particles formed during fast cooling and hence in an increase in hardness.

References

1. T. ISHII, H. YABE and A. KASHIWAZAKI, *Toshiba Rev.* **44** (1989) 875.
2. Y. C. HUANG, *J. Jpn. Inst. Metals* **23** (1984) 385.
3. J. MIZUKOSHI and E. TSUJI, Report of Industrial Technology Research Institute, No. 1 (Osaka Prefectural Industrial Research Institute, 1991) p. 38.
4. S. YAMADA, T. HAMADA, J. IMAI, E. TSUJI and T. MIZUKOSHI, *J. Jpn. Inst. Metals* **56** (1992) 247.
5. F. A. GOLIGHTLY, F. H. STOTT and G. C. WOOD, *J. Electrochem. Soc.* **126** (1979) 1035.
6. T. AMANO, S. YAJIMA and Y. SATO, *J. Jpn. Inst. Metals* **41** (1977) 1074.
7. G. A. GOLIGHTY, E. H. STOTT and G. C. WOOD, *Oxid. Metals* **10** (1976) 163.
8. J. K. TIEN and F. S. PETTET, *Metall. Trans.* **3** (1972) 1587.
9. H. OKABE, *J. Jpn. Inst. Metals* **50** (1986) 500.
10. E. TSUJI, *ibid.* **53** (1989) 1248.
11. K. MIZUUCHI, Y. OKADA, I. ONAKA and S. NENNO, *ibid.* **52** (1988) 878.

Received 2 July 1992
and accepted 27 April 1993